

# CASIMIR-LIFSHITZ FORCES

Yaroslav Aulin\*

Zernike Institute for Advanced Materials, University of Groningen,  
Nijenborgh 4, 9747 AG Groningen, the Netherlands

*Current review paper is focused on theoretical and experimental research in the area of Casimir- Lifshitz forces, the topic which “most researchers try to avoid rather than study” and the force “which is so weak it is almost undetectable”. An overview of Lifshitz theory for van der Waals/Casimir interactions has been given, as well as some results of it provided. The experimental difficulties while trying to precisely measure this kind of forces are mentioned and discussed. Particular attention is paid to the repulsive forces because of their chance to be utilized in novel nanoscale devices. The following types of repulsion are considered: in liquids, due to the geometrical effects, and in systems with metamaterials. Finally, potential applications are discussed, namely: gecko effect, quantum levitation, reduction of friction, elimination of stiction in NEMS/MEMS, etc.*

## Contents

- I. Introduction**
- II. Theory of Casimir-Lifshitz forces**
  - A. Molecular van der Waals forces and Hamaker theory**
  - B. Casimir effect for conducting surfaces in vacuum**
  - C. Lifshitz theory**
- III. Measurement of Casimir-Lifshitz forces**
- IV. Possibility of repulsion**
  - A. In liquids**
  - B. Geometrical effects**
  - C. Metamaterials**
- V. Prospective applications**
  - A. Gecko effect**
  - B. Prevention of stiction in MEMS/NEMS**
  - C. Quantum levitation**
  - D. The Casimir oscillator**
  - E. Reduction of friction**
- VI. Conclusions**
- Acknowledgements**
- References**

## I. Introduction

The phenomenon of attraction between molecules in a gas, or the van der Waals interaction, has been known since 1870s. Attraction between polar molecules was understood, however between non-polar ones it had remained a mystery until Fritz London used quantum theory to explain the existence of attractive forces by the means of zero-point fluctuations in the positions of charges inside the molecules or atoms [1].

In the end of 1930s it was already clear that the free energy of interaction of neutral molecules varies as the inverse sixth power of a distance, but by that time scientists were already interested in interactions between the objects of mesoscopic size (100nm-100 $\mu$ m), which are much larger than the atoms or molecules, for example: colloid particles in a solution, aerosols, surfaces and interfaces, thin films. In the 1940s Theo Overbeek and Evert Verwey, from Philips Laboratories in Eindhoven, were measuring the forces between small particles. Unexpectedly, the results of their experiments turned out to contradict the quantum mechanical theory of charge fluctuations developed by

---

\*email: y.aulin@student.rug.nl

London in the 1930s. At separations beyond a few nanometers the strength of interaction was decreased faster than it was expected [2-4]. Overbeek suggested that this difference was due to the finite speed of light, i.e. the retardation effects, but because of the lack of theoretical knowledge needed to tackle the problem he asked theoretical physicist Hendrik Casimir to investigate it. Casimir in collaboration with Dik Polder (both also from Philips Labs) successfully solved this task. In 1947 they developed a theory of London- van der Waals forces taking into account the retardation effects. The interaction of an atom and perfectly conducting plane, and the interaction between two atoms were considered [5]. Soon afterwards, Casimir proposed another interpretation of the results in terms of quantum vacuum fluctuations leading to his famous formula for the attraction force between two ideally conducting metal plates in vacuum. This phenomenon of attraction is nowadays widely known as the Casimir effect [6].

However, in reality no material behaves like a perfect conductor. The theory of Casimir was further extended by Lifshitz, Dzyaloshinskii and Pitaevskii for the general case of macroscopic bodies made of real materials and described in terms of their dielectric functions [7,8]. The Lifshitz's derivations are now considered as a masterpiece of theoretical physics. The theory is based on fluctuation-dissipation theorem and the assumption that the dielectric permittivities of the materials are known. It correctly describes the interaction that results from quantum fluctuations at an arbitrary separation covering both the long-range (Casimir) and the short range (van der Waals) modes. The weaker attraction at long range mode is called the Casimir or Casimir-Lifshitz force, although it is simply a modification of the van der Waals force. The theory of Lifshitz might be easily generalized for the cases of anisotropic materials, magnetic materials, and arbitrary geometries.

The experiments in the 1940s simply showed the existence of the force which falls off more rapidly than the van der Waals force. Several more decades of the experimentalists' efforts were needed in order for the Casimir force to be measured directly. That was finally done in 1978 by Overbeek [9] (who, by the way, also performed experiments with the colloids in the 1940s), when the force between a small metal sphere and a metal plate was detected, but these measurements lacked accuracy. Two more decades passed, and in 1997 the force between a gold-plated hemisphere and a gold plate attached to a torsion pendulum was measured with high precision by Steve Lamoureux [10].

The Casimir-Lifshitz interaction is starting to be more and more important due to the breakthrough in nanoscience and nanotechnology. It is of technological importance in MEMS/NEMS at the separations less than 200 nm.

Recently there has been a lot of interest to the repulsive Casimir-Lifshitz forces [11,12], once detected and precisely measured they would probably find some application in novel nano-scale devices, and might even cause a revolution and further level of miniaturization in nanomechanical systems.

In fundamental physics the Casimir effect also plays a crucial role, for instance in the search of hypothetical forces beyond the standard model [3,4].

In Section II an overview of the theory of van der Waals interaction is presented starting from non-retarded van der Waals interaction and Hamaker pairwise summation and ending with the Lifshitz theory. The original result of Casimir for perfectly conducting plates is also mentioned for the sake of illustration and due to historic reasons. Section III explains experimental methods and mentions the problems that are encountered on the way for precision measurement. Section IV is devoted to the repulsive interaction in different systems: in liquids, metallic surfaces with complicated geometries, and systems that

use metamaterials. Recent report on the experimental results of the repulsive force measurement by Munday et al. [12] is discussed, and problems associated with optical data descriptions are also shown. Section V contains the description and analysis of prospective applications in real devices.

## II. Theory of Casimir-Lifshitz forces

### A. Molecular van der Waals forces and Hamaker theory

The intermolecular potential of interaction of two uncharged molecules scales as the inverse-sixth power of the distance  $-C/r^6$ , where  $C$  is a positive coefficient. There exist three different types of interaction between molecular dipoles [1]: i) Keesom – between two permanent dipoles, ii) Debye – permanent dipole–induced dipole, iii) London – induced dipole–induced dipole, they all obey the inverse sixth power law. When the interacting objects are larger than molecules or atoms, a logical question of how to calculate the van der Waals forces between them arises. The simplest approach is the pairwise summation approximation proposed by Hamaker (Fig.1). Assuming that the infinitesimal parts of the bodies interact according to  $-C/r^6$  law, after performing summation over the volume of the bodies, one obtains the energy of interaction, for instance for parallel planar blocks it scales as the inverse square of separation ( $1/l^2$ ) and for the spheres as the inverse first power of separation ( $1/l$ ). However, as it was shown by Axilrod and Teller [13] the van der Waals forces are not additive, so in this case, the superposition principle breaks down and hence the result of the pairwise summation might be true only in some approximation. The most straightforward way to address the problem is to solve it using the electromagnetic boundary conditions.

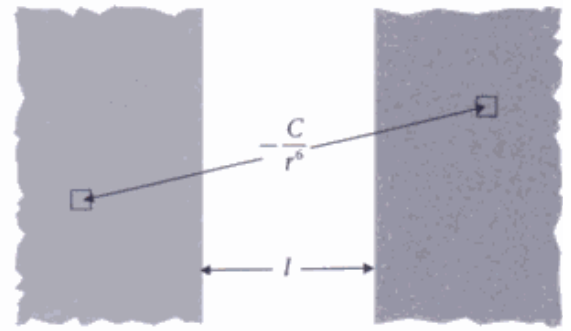


**Figure 1.** Pairwise summation over the volume of two planar blocks, the incremental parts of which interact according to inverse sixths power law [1].

Geometry	Free energy of interaction
“half spaces” at separation $l$	$-\frac{A_{Ham}}{12\pi l^2}$ per unit area
Sphere of radius $R$ near a planar thick wall at separation $l$	$l \ll R,$ $-\frac{A_{Ham}}{6} \frac{R}{l},$ per pair of bodies
Spheres of radii $R_1$ and $R_2$ near contact at separation $l \ll R_1, R_2$	$-\frac{A_{Ham}}{6} \frac{R_1 R_2}{(R_1 + R_2) l},$ per pair of spheres
Spheres of radius $R$ far apart at distance $z \gg R,$	$-A_{Ham} \cdot \frac{16}{9} \frac{R^6}{z^6},$ per pair of spheres

**Table 1.** Free energy of the van der Waals interaction for different geometries.

The coefficient of van der Waals interaction between large bodies is called a Hamaker constant  $A_{Ham}$  and is in the units of energy [1]. Examples for various geometries are shown in Table 1. The force of interaction between the bodies is obtained by taking a derivative of the free energy of interaction with respect to the separation.

### B. Casimir effect for conducting surfaces in vacuum

As it is known from quantum electrodynamics the zero point energy of fluctuating electromagnetic field in vacuum is given by the following expression

$$E = \frac{1}{2} \sum_i \hbar \omega_i, \quad (1)$$

where the sum is taken over all the frequencies of normal modes.

Following Casimir, consider two parallel perfectly conducting plates, which are grounded and charge-neutral [6] (Fig. 2). For this case the boundary condition is that the electric field equals zero at the surfaces of the plates. The introduction of the boundary condition leads to elimination of some normal modes from the sum in (1) and as a result to the change in the energy of vacuum fluctuations.

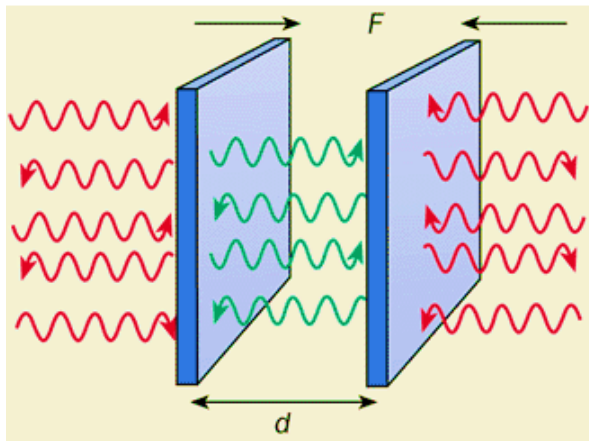


**Figure 2.** The Casimir effect for two perfectly conducting metallic plates [14].

This approach reduces complicated quantum electrodynamics problem to a much simpler classical electromagnetism problem. In order to obtain the force acting on the plates, one should take the derivative of zero-point energy with respect to the separation between the plates. Finally, the famous Casimir formula [6] for the force between two conductive plates is obtained:

$$F = -\frac{\pi^2}{240} \cdot \frac{\hbar c}{d^4} \cdot A, \quad (2)$$

where  $A$  is the surface area of the plate, and  $d$  is the separation. According to (2), the magnitude of the force per unit area is  $130 \text{ nN/cm}^2$  (what is equal to  $1.3 \cdot 10^{-8} \text{ bar}$  in terms of pressure) at the separation of  $1 \mu\text{m}$  [15], however if we calculate it at the separation of  $10 \text{ nm}$ , the force is  $100^4 = 10^8$  times bigger (!) and is equal to  $13 \text{ N/cm}^2$ , the corresponding pressure is equal to  $1.3 \text{ bar}$  (compare to  $1 \text{ atm} = 1.01325 \text{ bar}$ ).

The original result of Casimir can be generalized for the case of arbitrary geometries different from plane-parallel, although the problem here is the lack of theoretical tools, the appropriate choice and convergence of numerical methods for calculations. For an experimentally important case of a sphere and a plate of ideal materials the result may be obtained analytically and the expression for the force [16] looks like

$$F = -\frac{\pi^3 \hbar c}{360} \cdot \frac{R}{d^3}, \quad (3)$$

where  $R$  is the radius of the sphere and  $d$  is the separation between the sphere and the plate, provided it is much smaller than  $R$ .

### C. Lifshitz theory

The theory of Casimir was extended by Lifshitz and coworkers [7,8] for the case of real materials. The original derivations of Lifshitz were done for the bodies with planar geometry, however here we provide an overview of the outcomes of the theory for a plate and a sphere, the geometry convenient and widely used in the experiments.

For the interaction between the plate and the sphere of radius  $R$  at separation  $d$  in a medium the force can be written as [16]

$$F_{C-L}(d) = \frac{\hbar}{2\pi c^2} R \int_{\xi=0}^{\infty} \int_{p=0}^{\infty} \epsilon_3 p \xi^2 \left[ \ln \left( 1 - \Delta_{31}^{(1)} \Delta_{32}^{(1)} e^{-x} \right) + \ln \left( 1 - \Delta_{31}^{(1)} \Delta_{32}^{(1)} e^{-x} \right) \right] dp d\xi, \quad (4)$$

where we have for the Fresnel coefficients  $\Delta$ 's

$$\Delta_{3k}^{(1)} = \frac{s_k \epsilon_3 - s_3 \epsilon_k}{s_k \epsilon_3 + s_3 \epsilon_k}, \quad \Delta_{3k}^{(2)} = \frac{s_k - s_3}{s_k + s_3},$$

$$x = \frac{2d\sqrt{\epsilon_3}\xi p}{c}, \quad s_k = \sqrt{p^2 - 1 + \frac{\epsilon_k}{\epsilon_3}}, \quad (5)$$

$\hbar$  is the Planck's constant,  $c$  - the speed of light in vacuum, and  $\epsilon_1, \epsilon_2$ , and  $\epsilon_3$  are the dielectric functions of the sphere, the plate and intertwining medium respectively, evaluated at the imaginary frequencies according to

$$\epsilon_k \equiv \epsilon_k(i\xi) = 1 + \frac{2}{\pi} \int_0^\infty \frac{x \text{Im}[\epsilon_k(x)]}{x^2 + \xi^2} dx, \quad (6)$$

Surface roughness influences the Casimir-Lifshitz force. The modified formula including the roughness correction in the proximity force approximation can be written as

$$F_{C-L}^{rough}(d) = \sum_{i,j} \sigma_i^{(s)} \sigma_j^{(p)} F_{C-L} \left[ d - (\delta_i^{(s)} + \delta_j^{(p)}) \right], \quad (7)$$

where  $\sigma_i$  is the fraction of the surface area of the sphere (s) or plate (p) displaced at a distance  $\delta_i$  from an ideally smooth surface. The exact theory beyond the proximity force approximation and within the weak roughness approximation can be found in [15]. In practice for liquids, when there is not enough experimental data available for all the frequencies, the oscillator models are used to represent the dielectric function:

$$\epsilon(i\xi) = 1 + \sum_i \frac{C_i}{1 + (\xi/\omega_i)^2}, \quad (8)$$

where  $C_i$  is the oscillator strength of an  $i^{\text{th}}$  oscillator. As usual two or three oscillator models are used: UV – ultraviolet, IR- infrared, and sometimes MW – microwave. For the oscillator strengths the following relation should be satisfied:

$$\sum_i C_i = \epsilon_0 - 1, \quad (9)$$

where  $\epsilon_0$  is static dielectric permittivity.

The Lifshitz theory can be easily extended for the case of magnetic materials, and anisotropic materials [17].

Formally, the case of perfect conductors is obtained by letting the dielectric constant  $\epsilon$  in the Lifshitz theory approach infinity.

### III. Measurement of Casimir-Lifshitz forces

Precise measurement of Casimir forces is a difficult experimental task. The problems in the experiment are: small magnitude of the force and the rapid fall off of it with increasing separation between the surfaces, roughness, absolute distance determination, and precise alignment of the surfaces. So far, most measurements of the Casimir force were performed in the plate-sphere geometry to avoid complications with the plate-plate alignment.

The Casimir force was detected with high precision in 1997, by measuring the interaction between a gold hemisphere and a gold plate attached to a torsion pendulum [10]. A schematic of the apparatus used in the measurement is shown in Fig. 3, and details of the torsion pendulum are shown in Fig. 4.

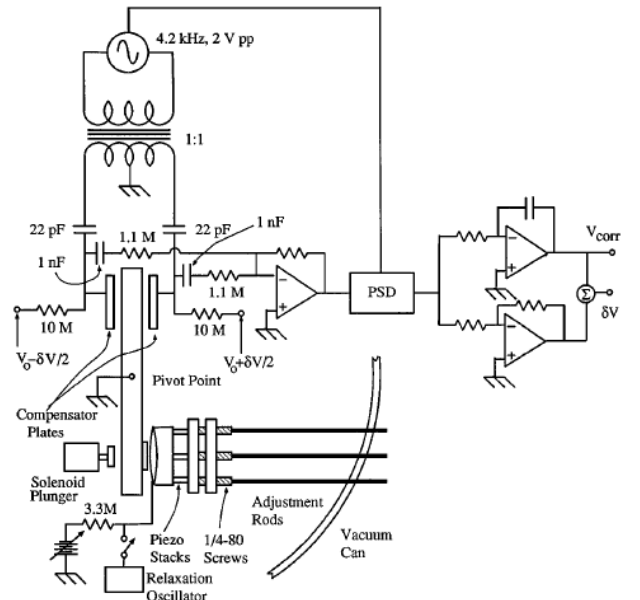


**Figure 3.** Schematic of the apparatus. The vacuum vessel dimensions are 55 cm diam by 110 cm tall. The solenoid activated plunger was used to press the plates

gently together (during alignment); after such pressing, the plates could be brought much closer [10].

The Casimir force plates used comprise a 2.54 cm diameter, 0.5 cm thick quartz optical flat, and a spherical lens with radius of curvature  $11.3 \pm 0.1$  cm and diameter 4 cm; each was coated by evaporation with a continuous layer of Cu of thickness 0.5 mm, on all surfaces. A layer of Au was then evaporated (0.5 mm thick) onto the faces which were subsequently brought together, as shown in Fig. 3, the flat electrode was mounted on one arm of the torsion pendulum, while the spherical electrode was placed on a

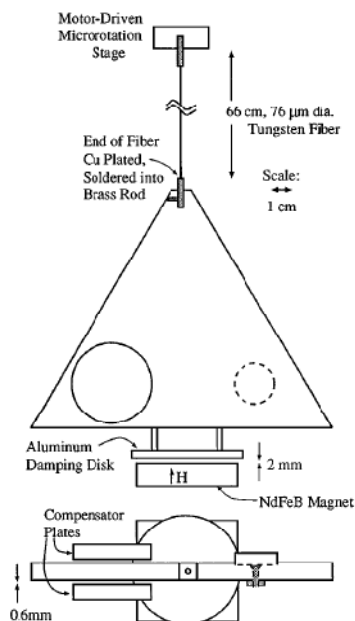


**Figure 4.** Details of the pendulum. The body has total mass 397 g. The ends of the W fiber were plated with a Cu cyanide solution; the fiber ends were bent into hairpins of 1 cm length and then soldered into a 0.5 mm diam, 7 mm deep holes in the brass rods. Flat-head screws were glued to the backs of the plates; a spring and nut held the plates firmly against their supports, and ensured good electrical contact [10].

micropositioning assembly. A vacuum of order 1024 torr was maintained to eliminate viscous effects. The results of the measurements using this method are shown in Fig. 5.

Other techniques for precision Casimir force measurements are: AFM (atomic force microscopy), measurements using MEMS (microelectromechanical systems), various torsional and spring-based methods.

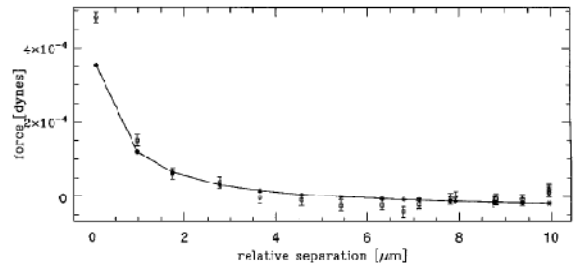


**Figure 5.** Measured force as a function of relative position using torsion pendulum technique [10].

Schematic representation of the experimental setup for AFM method is shown in Fig. 6. for measuring the force between a sphere made of material 1 and a plate of material 2 in a medium 3.

The sphere is attached to a conventional cantilever which is used for AFM imaging. Piezoceramics drives the cantilever towards the plate. The interaction between the sphere and the plate is detected by the motion of the cantilever. The deflection of the cantilever is monitored by the laser and a quadrant detector. The deflection obeys Hooke's

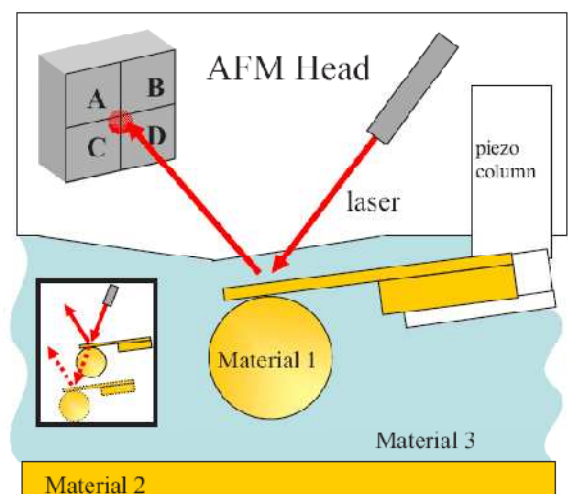


**Figure 6.** An experimental setup for the measurement of Casimir force between a sphere and a plate in liquid

using AFM technique, a laser light is reflected off the back of a microcantilever, on which a sphere is attached and metallized. The reflected beam is detected on a split quadrant photodetector, which monitors the cantilever's deflection caused by any vertical force [12].

law:  $F = -kd$ , where  $k$  is the stiffness of the cantilever and  $d$  is the displacement of the cantilever. Due to the fact that the voltage on the detector is proportional to the displacement of the cantilever, for the force we have:  $F = \alpha V_{\text{det}}$ , where  $V_{\text{det}}$  is the detector voltage and  $\alpha$  is a constant.

The authors of [18] proposed to use the inverse colloid probe force microscopy to measure the force between a sphere and the plane. In this method the sphere is located on a surface and the cantilever is planar as it is shown in Fig. 7.

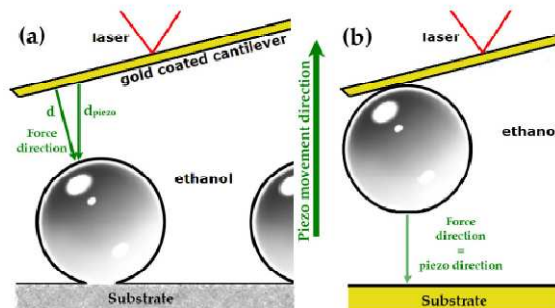


**Figure 7.** Measurement setup of the inverse colloid probe system (a) compared to a usual colloid probe system (b). Green arrows indicate the force direction in case of a sphere on a cantilever in (b), and in the case when the cantilever acts as a plate (a). Thus the plate is tilted with respect to the piezo movement in the inverse case. However, piezo movement defines the deflection sensitivity (nm/V), and thus the calibrated cantilever stiffness, which therefore is the same for both systems. Hence, the following corrections should be introduced:  $d = d_0 + d_{\text{piezo}} \cos(\alpha)$  and  $F = F_{\text{measured}} \cdot \cos(\alpha) - 1$  [18].

The method has several advantages: sticking spheres to the cantilever is time consuming and it is avoided in this way, measurements on multiple spheres of different size can be performed in a short time. The disadvantage of the method is the calibration of the system due to the fact that the force direction is different from vertical one (Fig. 7) in contrary to the usual colloid probe method. The images of the spheres on the plane and the profiles of surfaces are shown in Fig. 8.

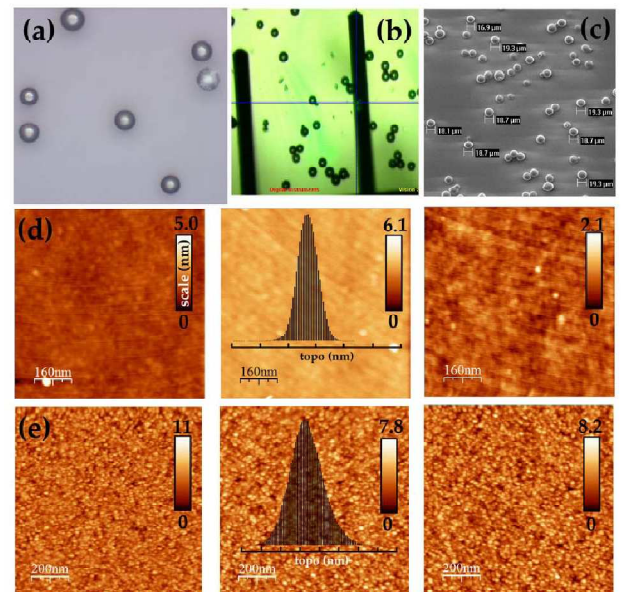


**Figure 8.** (a) Optical image of spheres sintered on the plate (b) Three cantilevers together with the spheres as seen from the top in AFM. (c) SEM measurement of the diameter of the spheres after sintering. (d) Topography AFM scans of a borosilicate sphere (the stripes are noise during imaging). (e) Topography AFM scans of the gold coated cantilever [18].

The experimental setup for the Casimir force measurement using MEMS is shown in Fig. 9. The device consists of polysilicon plate suspended on two of its opposite sides by thin horizontal rods. The sphere is attached to a piezo device.

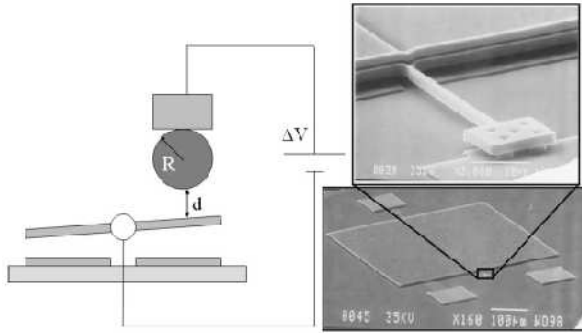


**Figure 9.** MEMS Casimir force detection setup. Schematic of the experiment (not to scale) and scanning electron micrographs of the micromachined torsional device used for the measurement of the Casimir force with a closeup of one of the torsional rods anchored to the substrate. As the metallic sphere approaches the top plate, the Casimir force causes a rotation of the torsional rod [19].

When the sphere is moved towards the plate, the plate rotates due to the Casimir force acting between the bodies. The force is detected by the measurement of the difference of the capacitances between the plate and two bottom electrodes.

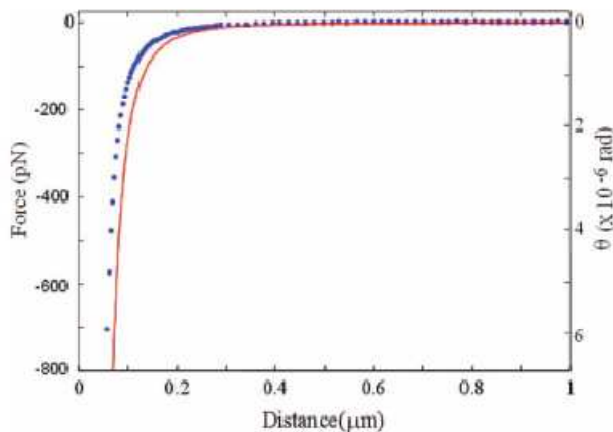


**Figure 10.** Experimental measurement of the Casimir force from the MEMS torsional device. Angle of rotation of the top plate in response to the Casimir force as a function of distance. (Red line) Predicted Casimir force without corrections for surface roughness or the finite conductivity. (Blue dots) Experimental results [19].

## IV. Repulsive forces

### A. In liquids

If we consider equation (4) we can see that under certain conditions the force is repulsive [1,12], this happens if

$$\begin{aligned} \epsilon_A > \epsilon_m > \epsilon_B \\ (\text{or } \epsilon_B > \epsilon_m > \epsilon_A) \end{aligned} \quad (10)$$

Examples of the systems that satisfy this condition are rare, however for short range van der Waals forces there is a well known experiment demonstrating the repulsive force: medium m is liquid Helium, B is the container, and A is air, for the permittivities of these media the condition mentioned above is fulfilled ( $\epsilon_{\text{wall}} > \epsilon_{\text{He}} > \epsilon_{\text{air}}$ ). As a result, liquid helium is crawling up the walls of the container.

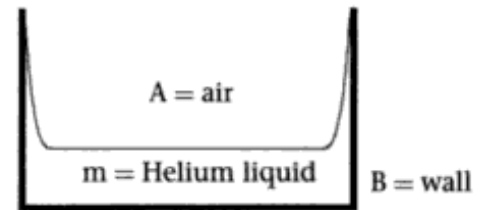


**Figure 11.** The crawling-the-walls experiment with liquid helium in a vessel demonstrating the repulsive van der Waals force. The polarizability of liquid helium is greater than that of air but less than that of the walls, as a result the liquid tries to put as much of itself as possible near solid walls to create an ever-thicker film to the extent that van der Waals energy can pay for this mass displacement against gravity [1].

For solid-liquid-solid system condition (10) is satisfied over a large frequency range for gold, bromobenzene and silica, the frequency dependences of the permittivities of these materials are shown in Fig. 12(b). According to the calculations of the authors in [12], this results in overall repulsive force between a golden sphere and a silica plate. In their calculations they used for gold the Drude model:

$$\varepsilon(\omega) = 1 - \frac{\omega_p^2}{\omega(\omega + i\gamma)} \quad (11)$$

where  $\omega_p = 7.5 \text{ eV}$  and  $\gamma = 0.061 \text{ eV}$ , even less data was available for bromobenzene and the two oscillator model was used:

$$\varepsilon(i\xi) = 1 + \frac{C_{IR}}{1 + \left(\frac{\xi}{\omega_{IR}}\right)^2} + \frac{C_{UV}}{1 + \left(\frac{\xi}{\omega_{UV}}\right)^2}. \quad (12)$$

with the values of the parameters:  $\omega_{IR} = 5.47 \times 10^{14} \text{ s}^{-1}$  and  $\omega_{UV} = 1.286 \times 10^{16} \text{ s}^{-1}$  - absorption frequencies,  $C_{IR} = 2.967$  and  $C_{UV} = 1.335$  - the corresponding absorption strengths.

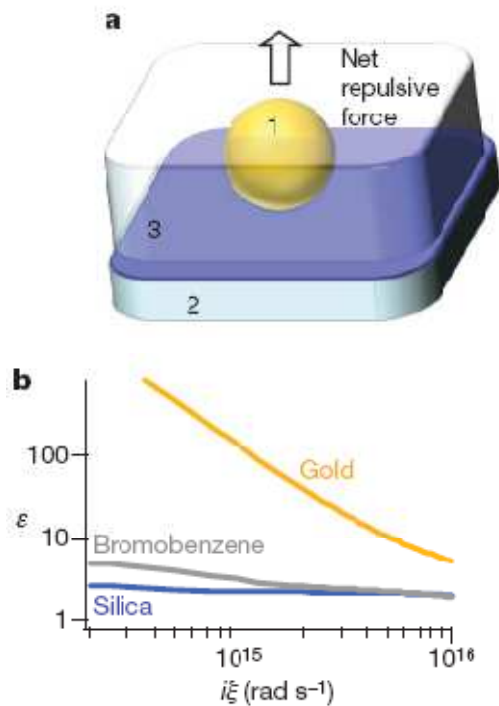


**Figure 12.** Repulsive quantum electrodynamic forces can exist for two materials separated by a fluid. *a*, The interaction between material 1 and material 2 immersed in a fluid (material 3) is repulsive when  $\varepsilon_1(i\xi) > \varepsilon_3(i\xi) > \varepsilon_2(i\xi)$ , where the  $\varepsilon(i\xi)$  terms are the dielectric functions at imaginary frequency. *b*, The optical properties of gold, bromobenzene and silica are such that  $\varepsilon_{\text{gold}}(i\xi) > \varepsilon_{\text{bromobenzene}}(i\xi) > \varepsilon_{\text{silica}}(i\xi)$  and

lead to a repulsive force between the gold and silica surfaces [12].

The measurements were performed in bromobenzene between a  $39.8 \mu\text{m}$  polystyrene sphere coated with  $100 \text{ nm}$  thick gold layer and a silica plate. The system is shown in Fig. 12 (a). The sphere was attached to a cantilever of an AFM. In the experiment the Casimir force may be masked by other effects, for example electrostatic forces. To ensure that the surface charge is small the electrostatic force microscopy was performed on the samples, and no evidence of excess charge accumulation was found.

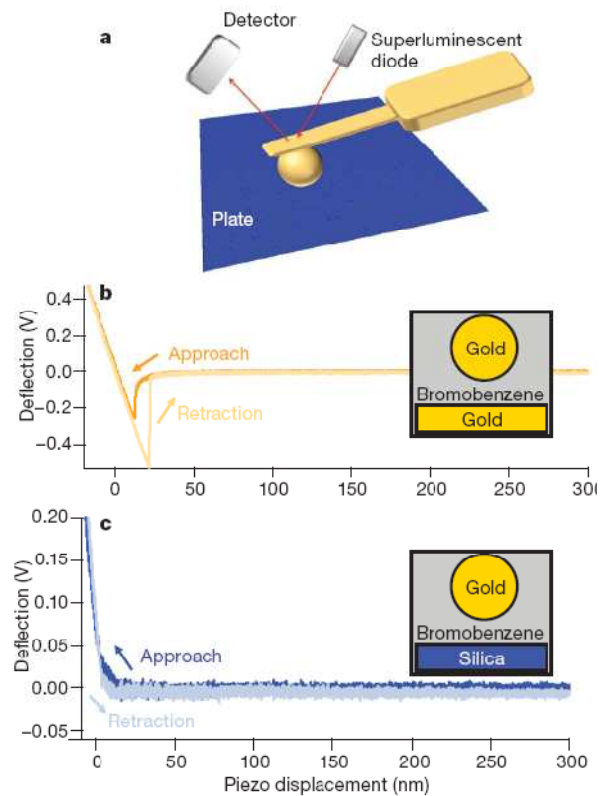


**Figure 13.** Experimental set-up and deflection data. *a*, A sphere is attached to an atomic force microscope cantilever, which is enclosed within a bromobenzene-filled cell for force measurements. *b*, Deflection data showing attractive interactions between a gold sphere and a gold plate. *c*, For the case of the same gold sphere and a silica plate, deflection data show a repulsive interaction evident during both approach and retraction. Note that the deflection voltage signal is a

difference signal obtained from the detector and is proportional to the bending of the cantilever [12].

Experimental data for the magnitude of the Casimir-Lifshitz force versus separation is provided in Fig. 14 for gold sphere and silica plate and for gold sphere and gold plate in bromobenzene.

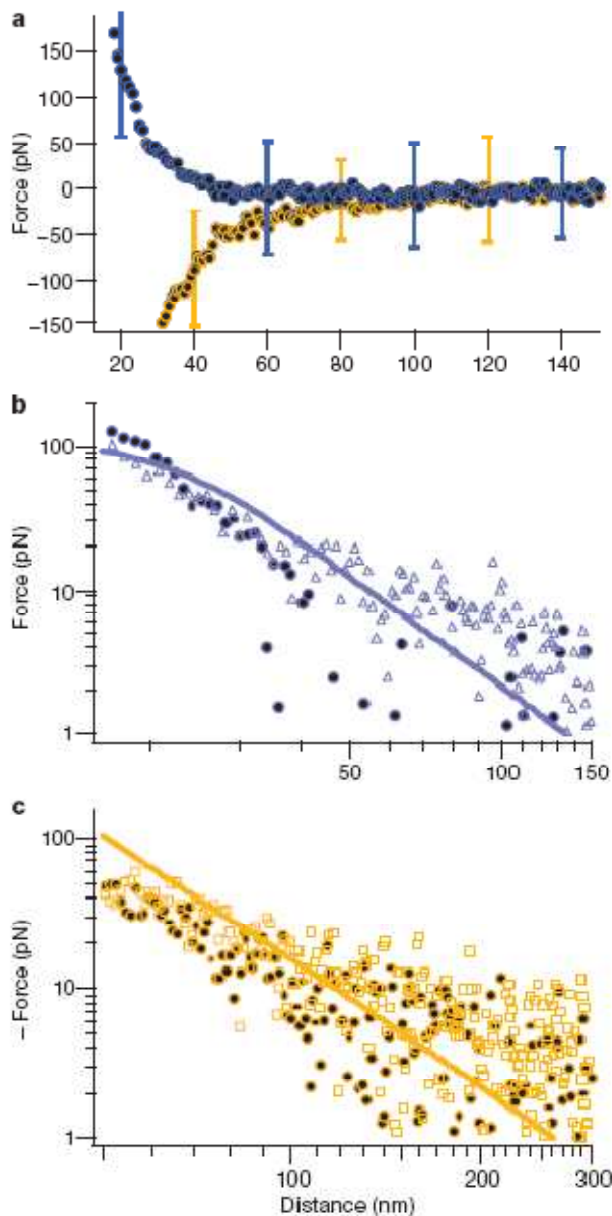


**Figure 14.** Attractive and repulsive Casimir-Lifshitz force measurements. *a*, Blue (orange) circles represent the average of 50 data sets for the force between a gold sphere and a silica (gold) plate in bromobenzene. For clarity, error bars, which represent the standard deviation of the data, are only shown for seven data

points. *b*, Measured repulsive force between a gold sphere and a silica plate in bromobenzene on a log-log scale (blue circles) and calculated force using Lifshitz's theory (solid line) including corrections for the measured surface roughness of the sphere and the plate. Blue triangles are force data for another gold sphere (nominally of the same diameter)/silica plate pair. *c*, Measured attractive force on a log-log scale for two gold sphere/plate pairs (circles and squares) in bromobenzene. The calculated force includes surface roughness corrections corresponding to the data represented by the circles [12].

However, the authors of [20] showed that the magnitude of the calculated force (and even sign) strongly depends on the oscillator model used for liquid medium. In Fig. 15 the results of calculations using Milling and Drummond & Chan oscillator models are compared.

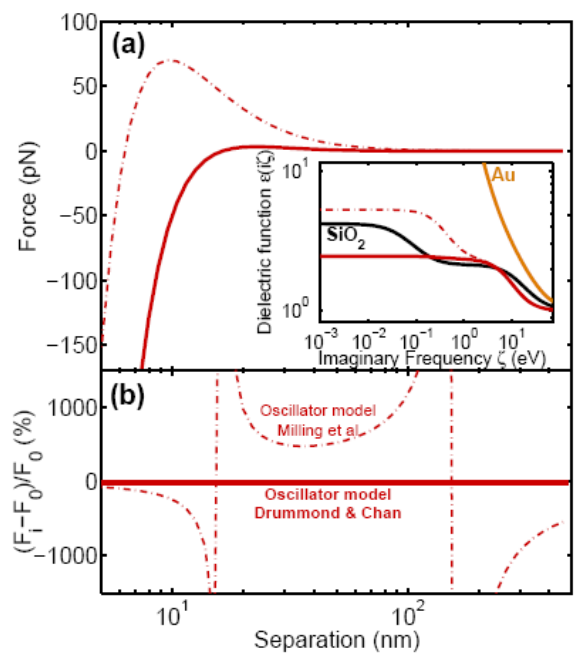


**Figure 15.** Comparison of the force calculated using Milling oscillator model with the force calculated using Drummond and Chan oscillator model for the gold-bromobenzene-silica system: (a) Calculated forces for gold-bromobenzene-silica using measured dielectric data for gold, silica and oscillator models for bromobenzene. The inset shows the dielectric function

of gold and silica together with the two oscillator models for bromobenzene. (b) The relative difference in force for the two oscillator models. The model of Drummond and Chan is used as a reference because it is better in the IR regime. Both models have almost the same UV oscillator strengths and frequencies, but these may not reflect the real dielectric response of bromobenzene in the UV regime. The force switches sign twice (attractive-repulsive-attractive) when using the model of Drummond et al [20].

Finally, we can conclude that the question whether the force in gold-bromobenzene-silica system is repulsive is not answered yet due to the lack of reliable experimental data (especially in the UV regime) for the dielectric permittivities of the materials, and because of the fact that the Casimir force might be masked by other interactions for example electrostatic which might also be repulsive.

## B. Geometrical effects

For the case of perfectly conducting plane parallel plates the Casimir force between them is always attractive, but it is possible for the force to be repulsive for other geometries. The concept is that the overall Casimir force is a sum of attractive contributions which lead to repulsion, i.e. the force acts to separate two structures. The prediction of Casimir forces in geometries different from plane parallel plates has had some problems due to the lack of appropriate theoretical tools and numerical methods.

It had been claimed that for a rectangular piston geometry – a box of size  $h \times b \times c$  with a partition at height  $a$  a repulsive force occurs provided that  $a/b > 0.785$ , however recent calculations [21] with the Green function method showed that the force is repulsive for Dirichlet and attractive for Neumann boundary conditions, and the resulting force turned out to be attractive.

The authors in [22] proposed to use the method of calculation for arbitrary geometries based on Maxwell stress tensor which has to be computed numerically via imaginary frequency Green's functions. As an example of a system with a repulsive force due to geometrical effects we consider here the 'zipper' geometry [22]. The structure consists of two metallic plates with brackets attached to them (Fig. 16). They are brought to a proximity in an interlocking fashion.

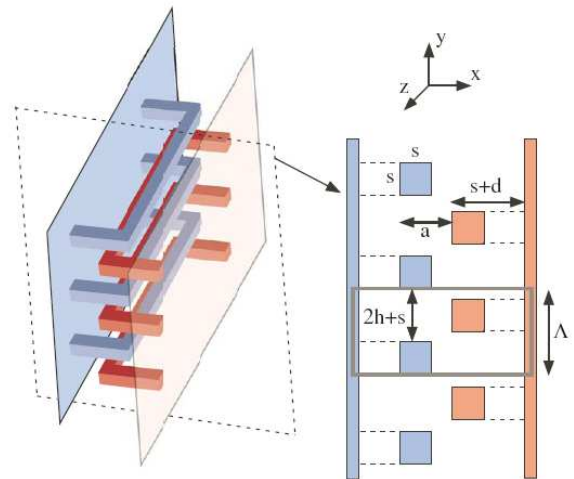


**Figure 16.** Three-dimensional schematic of the Casimir “zipper” geometry of interlocking metal brackets shown in different colors for illustration only, along with a two-dimensional  $xy$  cross section. The dashed lines extruding from the plates to the squares indicate their out-of-plane connectivity[22].

When the brackets are not interlocking the force is attractive. But when the plates move closer the dominant contribution to the force is due to the attraction between the brackets, which leads to repulsion between the structures when the brackets are interlocking. The force was computed numerically as a sum of the contributions of two polarizations: TE (transverse electric)- scalar magnetic field with Dirichlet boundary conditions and TM (transverse magnetic) – scalar electric field with Neumann boundary conditions. The contributions of the polarizations and the total pressure are shown in Fig.

17 as a function of separation between the plates  $a/s$  (for the case  $d/s = 2$  and  $h/s = 2$ ).

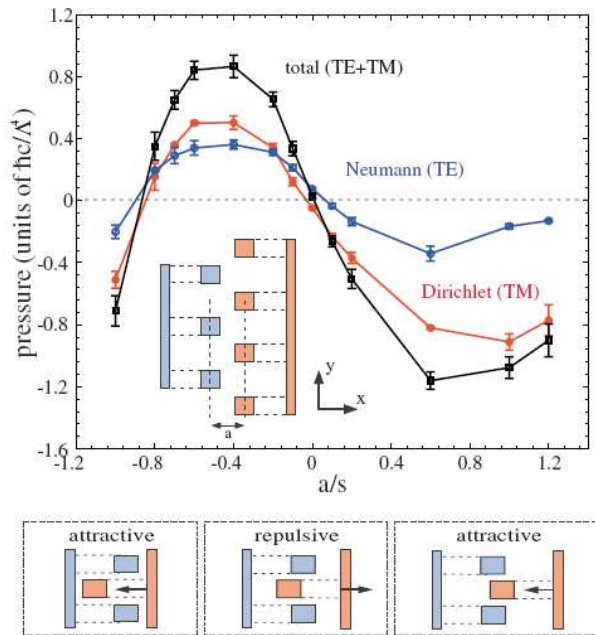


**Figure 17.** Top: Plot of the Neumann (blue, TE), Dirichlet (red, TM) and total (black, TE+TM) Casimir pressure between the objects of Fig. 16, as a function of  $a/s$ . The inset illustrates a two-dimensional cross section. Bottom: Schematic indicating the various qualitatively different Casimir force regimes between the two structures [22].

According to the calculations there are two equilibrium points:  $a/s = -0.8$  - unstable equilibrium and  $a/s = -0.01$  - stable equilibrium. The stability was determined with respect to lateral displacements. In between these points the force is repulsive.

However, it should be mentioned that the geometry considered is not easy to fabricate, and the effects of roughness, real material properties, and the alignment of the surfaces on the sign of the force have so far not been studied.

**C. Metamaterials**

In 1974 Boyer showed [23] that two parallel plates one of which is perfectly conducting and the other has infinite magnetic permeability repel each other due to

quantum fluctuations. The calculation using extended Lifshitz theory for the case of magnetic media shows that the repulsive forces can appear for the materials with high magnetic permeabilities, but this result was not considered seriously since for natural materials  $\mu(\omega)$  does not satisfy this condition. A solution is an evolving field of metamaterials [24,25] - artificial structures with designed electromagnetic properties. Metamaterials are composite materials with the inclusions of small size. At the wavelengths bigger than the inclusions' size the averaged permittivity and permeability are introduced to describe the interaction of the electromagnetic field with the structure. Metamaterials as usual have a narrow-band magnetic response. They also are anisotropic, and therefore the generalized Lifshitz theory for the case of magnetic anisotropic media should be used. Consider two anisotropic plates of metamaterials (Fig. 18, 19).

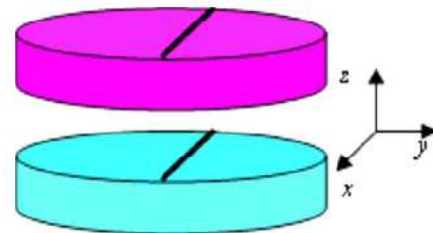


**Figure 18.** Two uniaxially parallel plates with diameter  $D$  and the thickness  $d$  in vacuum. The optic axes of the two plates are parallel to the  $x$  direction [26].

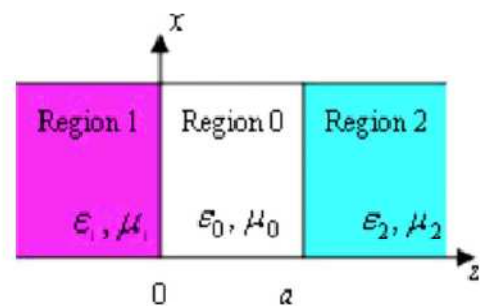


**Figure 19.** The cross section of the structure. Optical properties of the region  $i$  are described by

corresponding permittivity  $\varepsilon_i$  and permeability  $\mu_i$ , where  $i=0,1,2$  [26].

For the case of anisotropic media the permittivity and permeability are tensors. For uniaxial materials considered here the following matrices are introduced:

$$\varepsilon_i = \begin{pmatrix} \varepsilon_{i,\parallel} & 0 & 0 \\ 0 & \varepsilon_{i,\perp} & 0 \\ 0 & 0 & \varepsilon_{i,\perp} \end{pmatrix}, \quad \mu_i = \begin{pmatrix} \mu_i & 0 & 0 \\ 0 & \mu_i & 0 \\ 0 & 0 & \mu_i \end{pmatrix} \quad (13)$$

$i=1,2$

The resulting formula for Casimir-Lifshitz force versus separation reads

$$F(a) = -\frac{\hbar}{2\pi^2 c^3} \int_1^\infty p^2 dp \int_0^\infty \xi^3 d\xi \left[ \left( \frac{s_1 + \mu_1 p s_2 + \mu_2 p}{s_1 - \mu_1 p s_2 - \mu_2 p} e^{2\xi p a/c} - 1 \right)^{-1} + \left( \frac{s_1 + \varepsilon_1 \sqrt{1 + \delta_1} p s_2 + \varepsilon_2 \sqrt{1 + \delta_2} p}{s_1 - \varepsilon_1 \sqrt{1 + \delta_1} p s_2 - \varepsilon_2 \sqrt{1 + \delta_2} p} e^{2\xi p a/c} - 1 \right)^{-1} \right], \quad (14)$$

where  $s_i = \sqrt{p^2 - 1 + \mu_i \varepsilon_i}$ ,  $i=1,2$ , a variable  $\delta_i$  is defined according to  $\varepsilon_{i,\parallel} = (1 + \delta_i) \varepsilon_{i,\perp}$  and the notation  $\varepsilon_i \equiv \varepsilon_{i,\perp}$  is used.

A Drude-Lorentz model was used to describe the properties of the materials:

$$\varepsilon(i\xi) = 1 + \frac{\Omega_{pe}^2}{\omega_e^2 + \xi^2 + \gamma_e \xi}, \quad (15)$$

$$\mu(i\xi) = 1 + \frac{\Omega_{pm}^2}{\omega_m^2 + \xi^2 + \gamma_m \xi}. \quad (16)$$

In these representations  $\Omega_{pe}$  ( $\Omega_{pm}$ ) is the plasma frequency,  $\omega_e$  ( $\omega_m$ ) is the electric (magnetic) resonance frequency, and  $\gamma_e$  ( $\gamma_m$ ) is the electric (magnetic) discipation factor. For metals, it becomes Drude model

$$\varepsilon(i\xi) = 1 + \frac{\Omega_p^2}{\xi^2 + \gamma \xi}, \quad \mu(i\xi) = 1. \quad (17)$$

For a metallic based metamaterial, the permittivity is usually considered to be an ordinary Drude-Lorentz response with a small Drude background

$$\varepsilon(i\xi) = 1 + (1-f) \frac{\Omega_e^2}{\omega_e^2 + \xi^2 + \gamma_e \xi} + f \frac{\Omega_D^2}{\xi^2 + \gamma_D \xi}, \quad (18)$$

where  $\Omega_D$  and  $\gamma_D$  are Drude parameters of the metal in metamaterial, and the fill factor  $f$  represents the fraction of metal in the metamaterial.

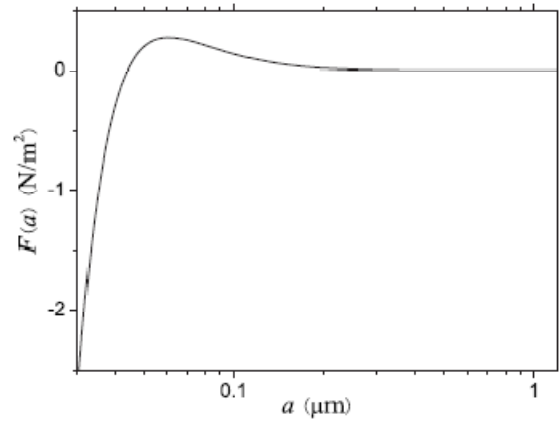


**Figure 20.** The Casimir force between a gold plate and an anisotropic gold-based metamaterial plate as a function of the separation  $a$ . The positive (negative) value corresponds to the repulsive (attractive) force.  $\Omega_p = \Omega = 1.38 \cdot 10^{16}$  rad / s is the gold plasma frequency.. Parameters used are  $\Omega_D = \Omega$ ,  $\gamma_m = \gamma_e = 0.005\Omega$ ,  $\gamma_D = \gamma = 0.004\Omega$ ,  $\Omega_e = 0.04\Omega$ ,  $\Omega_m = 0.009\Omega$ ,  $\omega_e = \omega_m = 0.1\Omega$ ,  $f_2 = 3 \cdot 10^{-5}$ ,  $\delta_2 = 0.001$  [26].

Another way to use metamaterials in order to achieve repulsion is as transformation media between two interacting objects. Consider a perfect lens – a slab of metamaterial with  $\varepsilon = \mu = -1$  of thickness  $b$

sandwiched between two perfectly conducting metal plates, at distance  $a$  between them (Fig. 21. (A) ).

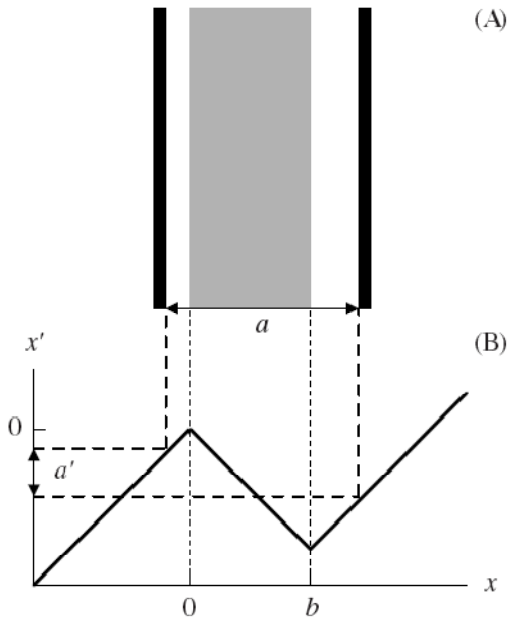


**Figure 21.** Casimir effect of left-handed metamaterials. (A) illustrates a material with  $\epsilon = \mu = -1$  sandwiched between two mirrors. (B) shows how the medium transforms the Casimir cavity of size  $a$  in physical  $x$  space into a cavity in  $x'$  space of size  $a'$  according to equation (2). The attractive Casimir force in  $x'$  space moves the mirrors further apart in  $x$  space: the Casimir effect in physical space is repulsive [27].

According to the theoretical approach developed in [27] the formula for the Casimir force remains the same as in the case of perfectly conducting plates, however the space is transformed by the metamaterial:

$$x' = \begin{cases} x, & \text{for } x < 0 \\ -x & \text{for } 0 \leq x \leq b \\ x - 2b & \text{for } x > b \end{cases} \quad (19)$$

Eq. (19) leads to the result that the force which is attractive in  $x$ -space (usual Casimir force between two plates without a metamaterial in between) is repulsive in  $x'$ -space (with the perfect lens).

## V. Prospective applications

### A. Gecko effect

The amazing ability of gecko, a small lizard that lives in warm countries, to walk across ceilings without the means of any sticky substance or mechanical device such as claws can be explained in terms of van der Waals forces [3,28]. Special structure of gecko's foot, which is shown in Fig. 22 at different scales, also makes it self-cleaning. By mimicking the adhesive pads of gecko's foot researchers are trying to develop re-adhesive surfaces with remarkable properties [29]. One of the examples of synthetic structures inspired by nature is a specimen of polydimethylsiloxane (PDMS) with mushroom structure shown in Fig. 23.

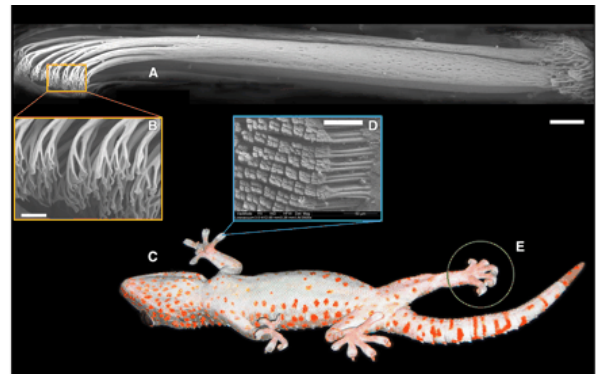


**Figure 22.** Gecko adhesive system. (A) Micrograph of a single gecko seta assembled from a montage of five Cryo-SEM images (B) Nanoscale array of hundreds of spatular tips of a single gecko seta. Note that the field of spatulae forms a plane at an acute angle to the base of the setal shaft. Raising the angle of the shaft above  $30^\circ$  may cause spatular detachment (C) Ventral view of a Tokay gecko (*Gekko gekko*) climbing a glass surface. (D) Array of setae are arranged in a nearly grid-like pattern on the ventral surface of each scansor. In this scanning electron micrograph, each diamond-shaped structure is the branched end of a group of four setae clustered together in a tetrad. (E) Toe peeling (digital hyperextension, DH) during detachment. Scale bars,  $50 \mu\text{m}$  (D),  $5 \mu\text{m}$  (A),  $1 \mu\text{m}$  (B) [28].

The specimen was fabricated using photolithographic technique.

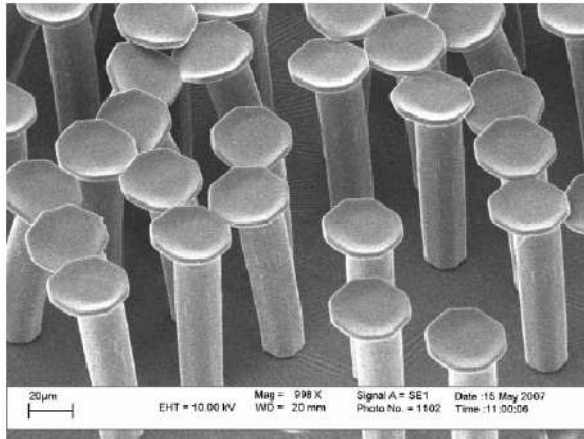


**Figure 23.** Example of a mushroom headed PDMS specimen. The hairs are approximately  $100\ \mu\text{m}$  long and  $20\ \mu\text{m}$  in diameter, the head thickness is  $3\ \mu\text{m}$ , head diameter  $40\ \mu\text{m}$  [29].

Adhesion strength measurements were performed for samples with pillar structure and mushroom structure. Maximum loads were recorded for the mushroom shaped specimen on a glass surface with strength of up to  $220\text{kPa}$  [29]. The structures also exhibited superhydrophobic properties. The experiments showed that simply washing with water could recover adhesion strength after contamination with dust.



**Figure 24.** Superhydrophobic synthetic Geckopad specimen. Note the small water droplet on the right of the image which is almost circular. The large drop has a diameter of approximately  $7\ \text{mm}$  [29].

This self-cleaning behavior is as well observed in some biological systems, most notably in lotus leaves, and is

hence termed the “lotus” effect. This is a natural cleaning mechanism whereby mud, tiny insects, and contaminants are swept away by water droplets rolling off the leaf surface without the leaf getting wet.

Another illustrative example of the research in the field of superadhesive tapes is [30], the researchers fabricated an array of polyimide hairs (Fig. 25) and studied the adhesive properties of the structure.

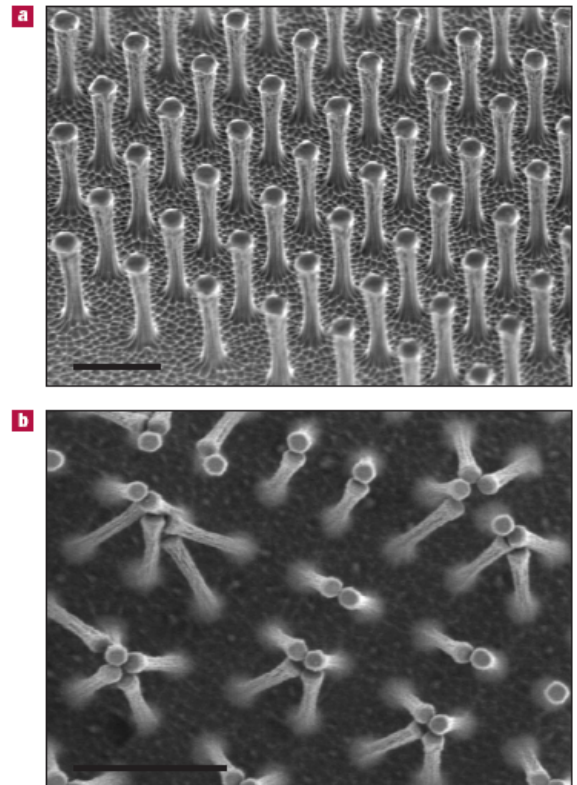


**Figure 25.** Scanning electron micrographs of microfabricated polyimide hairs. **a**, A small area near the edge of a  $1\ \text{cm}^2$  array of polyimide hairs. This array was later used to evaluate macroscopic adhesive properties of the mimetic material. **b**, Bunching is found to be one of the mechanisms responsible for the reduction of adhesive strength of the artificial hair. This micrograph also demonstrates the high flexibility of polyimide pillars. Both scale bars are  $2\ \mu\text{m}$  [30].

Significant difference of this structure from that one studied in [29] is that the size of the hairs in [30] was in the nanometer range. However, smaller size of the hairs lead to the problem with bunching, and hence the

reduction of adhesive strength. The experimental data on adhesive properties are provided in Figs. 26, 27.

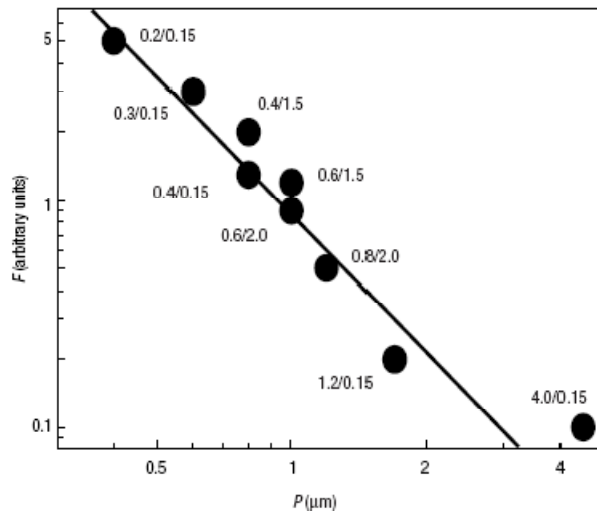


**Figure 26.** The perpendicular force  $F$  required for detaching various samples of polyimide hairs from a silicon surface. The experimental points are marked by  $D/H$ , indicating the hairs' diameters  $D$  and heights  $H$ , respectively. The solid curve is the best fit to  $F \propto P^{-2}$ . [30].

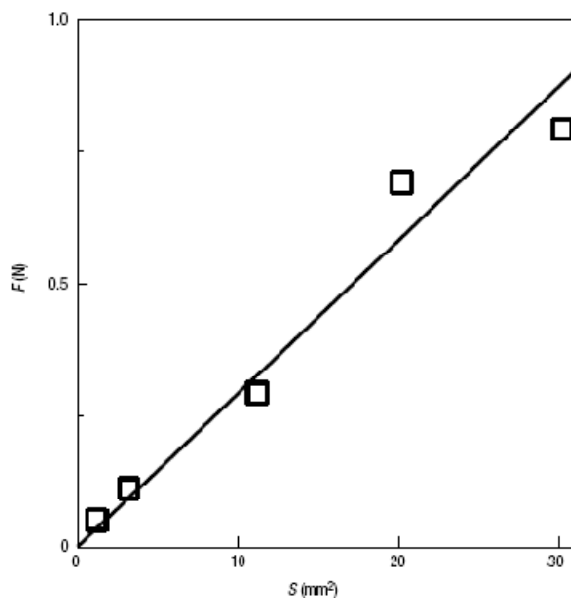


**Figure 27.** The adhesive force  $F$  exhibited by 'gecko tape' as a function of contact area  $S$ . Squares are experimental data; the solid line is the best linear fit [30].

An illustrative example of application of the new superadhesive materials is shown in Fig. 28.



**Figure 28.** Re-attachable dry adhesives based on the gecko principle can find a variety of applications. The photo illustrates this point by showing a spider-man toy clinging with one of its hands to a horizontal glass plate. The toy (15 cm high; weighing 40 g) has its hand covered with the microfabricated gecko tape, which provides  $a \approx 0.5 \text{ cm}^2$  contact with the glass and a carrying capacity of  $>100 \text{ g}$ . Note that the toy was already re-attached several times to various surfaces before this photo was taken [30].

### B. Prevention of stiction in MEMS/NEMS

The undesirable consequence of the Casimir effect is stiction due to attractive nature of the force [31]. It leads to the collapse of MEMS devices (Fig. 29, 30) when the surfaces are close enough, at the separations when the Casimir force starts to be important, and hence it prevents further miniaturization of the devices.

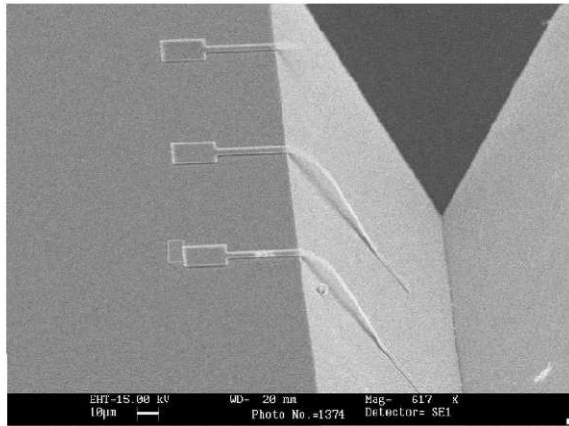


**Figure 29.** Stiction of microcantilevers to a substrate [31].

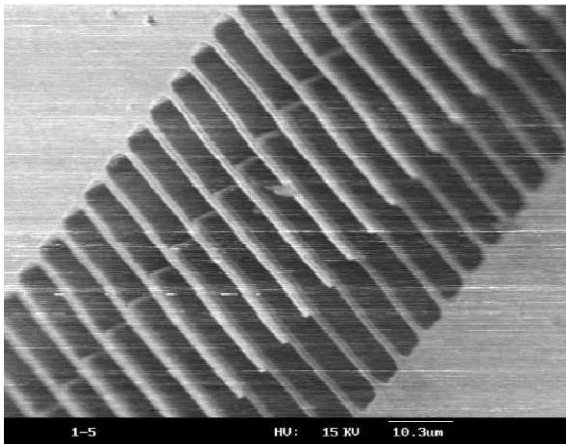


**Figure 30.** Adhesion between fingers of a comb structure in a microaccelerometer [31].

Repulsive forces could become a solution to the problem of stiction and lead to the next level of miniaturization in MEMS/NEMS.

### C. Quantum levitation

Repulsive Casimir-Lifshitz forces could also lead to a new phenomenon – so-called ‘Casimir levitation’- the case when repulsive force balances the gravitational one and as a consequence the object is levitated [19].

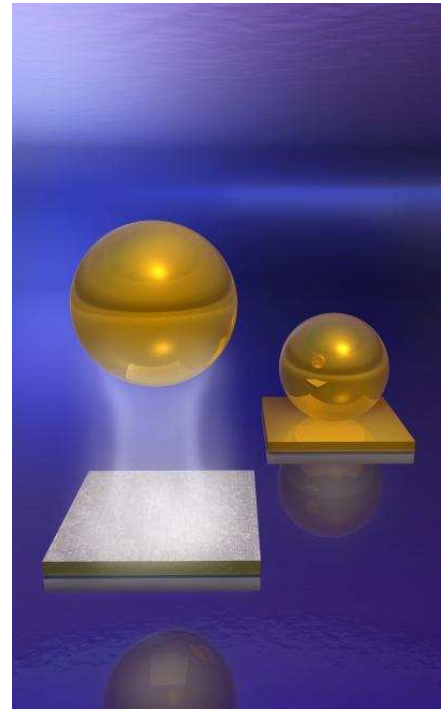


**Figure 31.** The artist's rendition of how the repulsive Casimir-Lifshitz force between suitable materials in a fluid can be used to levitate a small object of density greater than the liquid. Figures are not drawn to scale. Foreground: a gold sphere, immersed in bromobenzene, levitates above a silica plate. Background: when the plate is replaced by one of gold levitation is impossible because the Casimir-Lifshitz force is always attractive between identical materials. (Courtesy of the lab of Federico Capasso, Harvard School of Engineering and Applied Sciences)

There has been a number of proposals of mechanical devices based on the levitation effect. A mechanical sensor of small magnetic field or nano-compass is shown in Fig. 32. It consists of a ferromagnetic disk immersed in a fluid. A repulsive Casimir force exists between the disk and the plate, due to this force the disk is suspended and the gravitational force is compensated reducing losses and increasing the sensitivity of the device.

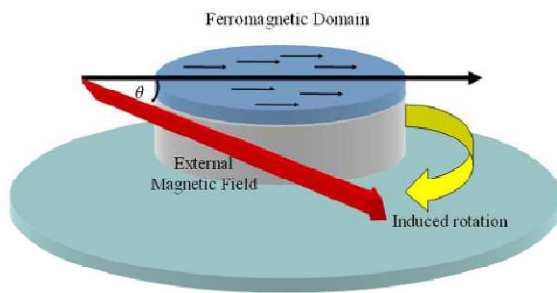


**Figure 32.** Floatation device based on Casimir-Lifshitz forces. A repulsive force develops between the disk immersed in a fluid and the plate, which is balanced by gravity. The nano-compass that could be developed to mechanically sense small magnetic fields [19].

Another idea is to use anisotropic materials. In this case the electromagnetic fields depend on the relative orientation of the optical axes of the interacting bodies. This leads to a torque which tends to align the bodies in order to minimize the system's energy. Consider a birefringent disk which levitates above the birefringent plate (Fig. 33).

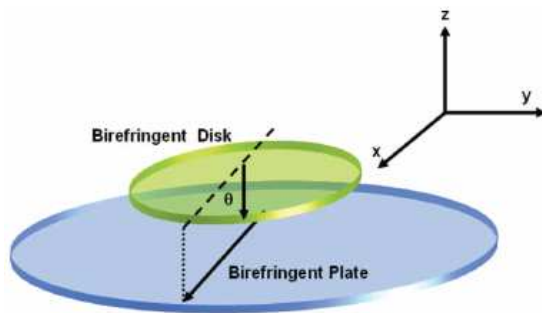


**Figure 33.** A torque develops between two birefringent parallel plates with in-plane optical axis when they are placed in close proximity [19].

If the optical axes of the materials are aligned the energy is minimal and the torque is equal to zero, however for an arbitrary angle  $\theta$  between the optical axes it varies as

$$M = A \sin(2\theta), \quad (20)$$

where  $A$  is proportional to the surface area and decreases with increasing surface separation. The

torque is maximal at  $\theta = \pi/4$ . Calculated values of the torque at different angles for a  $40\mu\text{m}$  in diameter calcite disk above a barium titanate plate at a distance of  $100\text{nm}$  in ethanol are shown in Fig 34 (a). Dependence of the repulsive force between the disk and the plate versus surface separation is shown in Fig. 34 (b). The equilibrium separation at which the quantum electrodynamic force balances the gravitation is approximately equal to  $100\text{nm}$ .

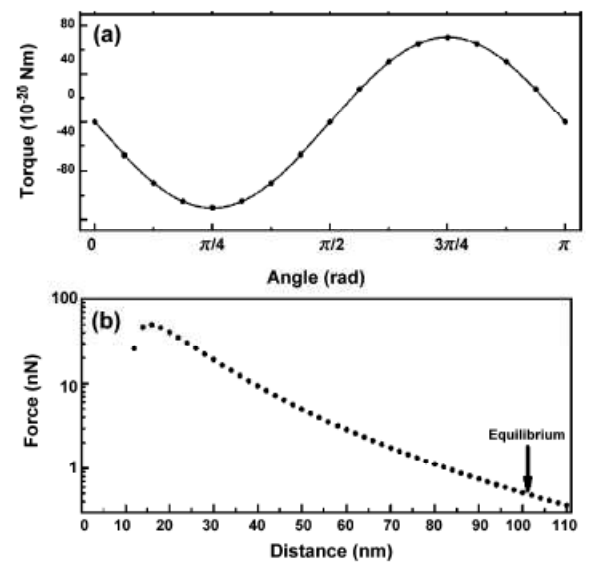


**Figure 34.** (a) Calculated torque as a function of angle between a  $40\mu\text{m}$  diameter disk made of calcite and a barium titanate plate separated in vacuum by a distance  $d = 100\text{nm}$ . The lines represent a fit with (20). (b) Calculated retarded van der Waals force as a function of plate separation for this system at a rotation angle of  $\pi/4$ . The arrow represents the distance at which the retarded van der Waals repulsion is in equilibrium with the weight of the disk [19].

The experimental implementation of this idea is not so simple because of the problems with the parallel alignment of the surfaces. At finite temperatures for small disks the Brownian motion will also play role and will result in translation and rotation. The probability to observe the angle  $\theta$  in thermal equilibrium is given by

$$p(\theta) \propto \exp\left(-\frac{U(\theta)}{k_B T}\right), \quad (21)$$

where  $U(\theta)$  is the energy associated with the torque and  $T$  is the temperature.

#### D. The Casimir Oscillator

Casimir interactions have a profound effect not only on static, but as well on the dynamic properties of micro- and nanostructures [19]. As an example consider a system which is called the Casimir oscillator (Fig. 35).

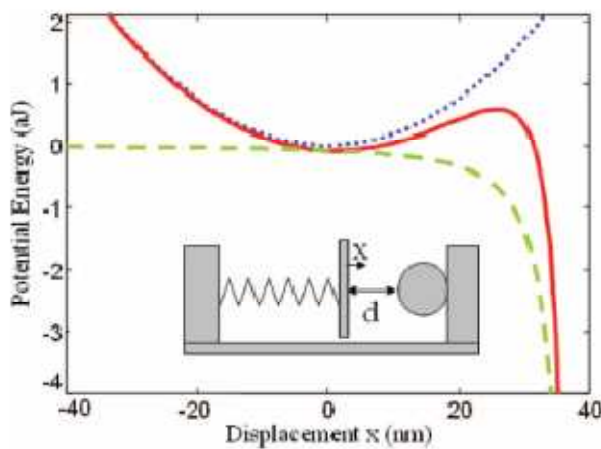


**Figure 35.** Simple model of the nonlinear Casimir oscillator (not to scale) (inset). Elastic potential energy of the spring (dotted line, spring constant  $0.019 \text{ Nm}^{-1}$ ), energy associated with the Casimir attraction (dashed line), and total potential energy (solid line) as a function of plate displacement. The distance  $d$  between the sphere ( $100 \mu\text{m}$  radius) and the equilibrium position of the plate in the absence of the Casimir force is chosen to be  $40 \text{ nm}$  [19].

A simple model of the Casimir oscillator consists of a movable metallic plate subjected to the restoring force of a spring obeying Hooke's law and the nonlinear Casimir force arising from the interaction with a fixed metallic sphere (Fig. 35 inset). For separations  $d$  larger than a critical value, the system is bistable: the potential energy consists of a local minimum and a global minimum separated by a potential barrier. The

local minimum is a stable equilibrium position, about which the plate undergoes small oscillations. The Casimir force modifies the curvature of the confining potential around the minimum, thus changing the natural frequency of oscillation and also introduces high order terms in the potential, making the oscillations anharmonic [32].

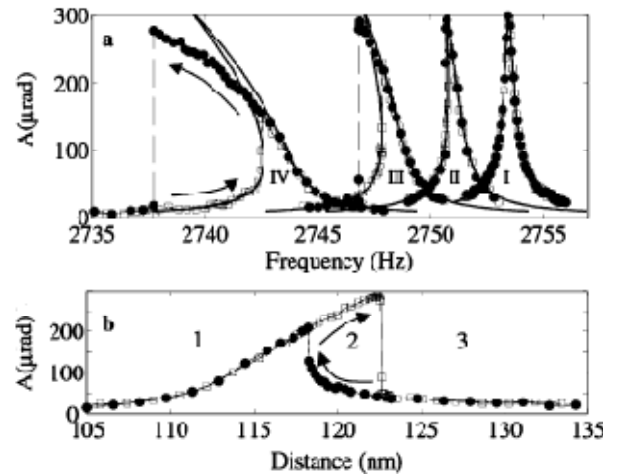


**Figure 36.** (a) Hysteresis in the frequency response induced by the Casimir force on an otherwise linear oscillator. Hollow squares (solid circles) are recorded with increasing (decreasing) frequency. (Solid lines) The predicted frequency response of the oscillator. The distance  $d$  between the oscillator and the sphere is  $3.3 \mu\text{m}$ ,  $141 \text{ nm}$ ,  $116.5 \text{ nm}$ , and  $98 \text{ nm}$  for peaks I, II, III, and IV, respectively. The excitation amplitude is maintained constant at  $55.5 \text{ mV}$  for all four separations. The solid lines are the calculated response. The peak oscillation amplitude for the plate is  $39 \text{ nm}$  at its closest point to the sphere. (b) Oscillation amplitude as a function of distance with excitation frequency fixed at  $2748 \text{ Hz}$  [32].

#### E. Reduction of friction

Another possible application of the repulsive Casimir force is the elimination of friction between moving surfaces [19], however it has been shown [33] that a new type of dissipative forces or so called 'Casimir friction' can arise due to the coupling of virtual photons to acoustic phonons in the material. According

to the theoretical predictions [33], the behavior of the frequency with shear velocity is determined by the frequency dependence of the reflectivity.

## VI. Conclusions

Casimir-Lifshitz interactions are significant in magnitude at separations of surfaces smaller than 100 nm, and play crucial role in nanomechanical systems. However, due to the complexity of their nature, weak magnitude and the lack of experimental techniques for studying them, a lot still remains unknown in the field.

Currently, the main problems with theoretical and experimental investigation of the Casimir-Lifshitz forces are: i) pairwise summation approach as usual breaks down, hence the force is non-additive. This complicates prediction of Casimir force for arbitrary non-standard geometries; ii) real surfaces are rough, which has to be taken into account; iii) Material properties  $\epsilon(\omega)$  and  $\mu(\omega)$  are not well known over all the range of frequencies for real materials, and appropriate approximations of them have to be made during theoretical calculations, as well as the experimental techniques of determination of the material properties in different frequency bands with reasonable accuracy should be developed; iv) nowadays the measurement of Casimir force with high precision is a challenge for the experimentalists due to the small magnitude, and the number of significant effects (roughness, optical properties, varying contact potentials, etc.) influencing the interaction. As a result new techniques of precise measurement are required. One of the prospective applications of attractive Casimir-Lifshitz forces is the gecko effect (superadhesive tapes), repulsive forces are likely to have more applications, however, the problem of repulsive forces is far from being solved, on the way there are both theoretical and experimental obstacles to be overcome. Once detected and precisely measured the repulsive forces would find a variety of practical

applications as for example prevention of stiction in MEMS(NEMS), reduction of friction in mechanical systems, Casimir levitation. Due to their incredible importance for the development of NEMS and the next level of miniaturization, future research should involve probing of Casimir-Lifshitz interactions between different materials which are prospective candidates for the repulsion.

## Acknowledgements

I am very grateful to my supervisor in the paper project Dr. George Palasantzas for providing some useful references, productive discussions, and review of my paper.

## References

1. V.A. Parsegian, "Van der Waals forces: A handbook for biologists, chemists, engineers, and physicists", Cambridge univ. press, 2006.
2. P. Ball, "Fundamental physics: Feel the force", Nature, 447 (2007).
3. S.K. Lamoureaux, "Casimir forces: Still surprising after 60 years", Phys. Today, 2 (2007).
4. A. Lambrecht, "The Casimir effect: a force from nothing", <http://physicsworld.com/> (2002).
5. H.B.G. Casimir, D. Polder, "The influence of retardation on the London-van der Waals forces", Phys. Rev. 73, 4 (1948).
6. H.B.G. Casimir, "On the attraction between two perfectly conducting plates" Proc. K. Ned. Akad. Wet. 51, 793 (1948).
7. E. M. Lifshitz, "The Theory of Molecular Attractive Forces", Sov. Phys. JETP 2, 73 (1956).
8. I.E. Dzyaloshinskii, E. M. Lifshitz, and L.P. Pitaevskii, "General theory of van der Waals' forces", Sov. Phys. JETP 10, 161 (1960).
9. P.H.G.M. van Blokland, J.T.G Overbeek, "Van der Waals Forces Between Objects Covered with a

- Chromium Layer”, *J. Chem. Soc. Faraday Trans. I*, 74, 11 (1978).
10. S.K. Lamoureux, “Demonstration of the Casimir Force in the 0.6 to 6  $\mu\text{m}$  Range”, *Phys. Rev. Lett.* 78 (1997).
11. S.K. Lamoureux, “Quantum force turns repulsive”, *Nature* 457(2009).
12. J.N. Munday, F. Capasso, and V.A. Parsegian, “Measured long-range repulsive Casimir-Lifshitz forces” *Nature*, 457 (2009).
13. B.M. Axilrod, E. Teller, “Interaction of the van der Waals type between three atoms”, *J. Chem. Phys.* 11 (1943).
14. <http://palasantzas.fmns.rug.nl/casimir.htm>
15. P.A. Maia Neto, A. Lambrecht, and S. Reynaud, “Roughness correction to the Casimir force: Beyond the Proximity Force Approximation”, *Europhys. Lett.*, 69, 6 (2005).
16. J.N. Munday and F. Capasso, “Precision measurement of the Casimir-Lifshitz force in a fluid”, *Phys. Rev. A* 75(2007).
17. C.G. Shao, D.L. Zheng, and J. Luo, “Repulsive Casimir effect between anisotropic dielectric and permeable plates” *Phys. Rev. A* 74, (2006).
18. P.J. van Zwoll, G. Palasantzas, J.Th.M. DeHosson, “Weak dispersive forces between glass-gold macroscopic surfaces in alcohols”, *Phys. Rev. E*, 79 (2009).
19. F. Capasso, J.N. Munday, D. Iannuzzi, and H. B. Chan, “Casimir Forces and Quantum Electrodynamical Torques: Physics and Nanomechanics”, *IEEE J. Select. Top. Quantum Electr.* 13 (2007).
20. P.J. van Zwoll, G. Palasantzas, J.Th.M. DeHosson, “The influence of dielectric properties on van der Waals/Casimir forces in solid-liquid systems”, *Phys. Rev. B* 79, 195428 (2009).
21. M. P. Hertzberg, R.L. Jaffe, M. Kardar, and A. Scardicchio, “Casimir forces in a piston geometry at zero and finite temperatures”, *Phys. Rev. D* 76, (2007).
22. A.W. Rodriguez, J.D. Joannopoulos, and S.G. Johnson, “Repulsive and attractive Casimir forces in a glide-symmetric geometry”, *Phys. Rev. A* 77, 062107 (2008)
23. T.H. Boyer, “Van der Waals forces and zero-point energy for dielectric and permeable materials”, *Phys. Rev. A* 9, 5(1974).
24. I.G. Pirozhenko, A. Lambrecht, “Casimir repulsion and metamaterials” *IOP J. Phys. A: Math. Theor.* 41, (2008).
25. F.S.S. Rosa, D.A.R. Dalvit, and P.W. Milonni, “Casimir-Lifshitz Theory and Metamaterials”, *Phys. Rev. Lett.* 100, 183602 (2008).
26. G. Deng, Z.Z. Liu, and J. Luo, “Attractive-repulsive transition of the Casimir force between anisotropic plates”, *Phys. Rev. A* 78, (2008).
27. U. Leonhardt and T.G. Philbin, “Quantum levitation by left-handed metamaterials”, *New J. of Phys.* 9 (2007).
28. K. Autumn, A. Dittmore, D. Santos, M. Spenko, and M. Cutkosky, “Frictional adhesion: a new angle on gecko attachment”, *J. of Exp. Biol.*, 209 (2006).
29. J. Davies, S. Haq, T. Hawke, and J.P. Sargent, “A practical approach to the development of a synthetic Gecko tape”, *Int. J. of Adhesion & Adhesives*, 29 (2009).
30. A. K. Geim, S. V. Dubonos, I. V. Grigorieva, K. S. Novoselov, A. A. Zhukov, and S. Yu. Shapoval, “Microfabricated adhesive mimicking gecko foot-hair”, *Nature Materials* 2, 461 - 463 (2003).
31. Y.P. Zhao, L.S. Yang, and T.X. Yu, “Mechanics of adhesion in MEMS — a review”, *J. Adhesion Sci. Technol.*, 17, 4 (2003).
32. H.B. Chan, V.A. Aksyuk, R.N. Kleiman, D.J. Bishop, and F. Capasso, “Nonlinear Micromechanical Casimir Oscillator”, *Phys. Rev. Lett.* 87, 21 (2001).
33. M. Kardar, R. Golestanian, “The “friction” of vacuum, and other fluctuation-induced forces”, *Rev. of Mod. Phys.*, 71, 4 (1999).